



10-5-2016


Frontal plane stabilization and hopping with a 2DOF tail

Garrett Wenger
University of Pennsylvania

Avik De
University of Pennsylvania

Daniel E. Koditschek
University of Pennsylvania, kod@seas.upenn.edu

Follow this and additional works at: https://repository.upenn.edu/e_se_papers

 Part of the [Electrical and Computer Engineering Commons](#), and the [Systems Engineering Commons](#)

Recommended Citation

Garrett Wenger, Avik De, and Daniel E. Koditschek, "Frontal plane stabilization and hopping with a 2DOF tail", *2016 IEEE/RSJ International Conference on Intelligent Robots and Systems (IROS)*. October 2016.

This paper is posted at ScholarlyCommons. https://repository.upenn.edu/e_se_papers/851
For more information, please contact repository@pobox.upenn.edu.

Frontal plane stabilization and hopping with a 2DOF tail

Abstract

The Jerboa, a tailed bipedal robot with two hip-actuated, passive-compliant legs and a doubly actuated tail, has been shown both formally and empirically to exhibit a variety of stable hopping and running gaits in the sagittal plane. In this paper we take the first steps toward operating Jerboa as a fully spatial machine by addressing the predominant mode of destabilization away from the sagittal plane: body roll. We develop a provably stable controller for underactuated aerial stabilization of the coupled body roll and tail angles, that uses just the tail torques. We show that this controller is successful at reliably reorienting the Jerboa body in roughly 150 ms of freefall from a large set of initial conditions. This controller also enables (and appears intuitively to be crucial for) sustained empirically stable hopping in the frontal plane by virtue of its substantial robustness against destabilizing perturbations and calibration errors. The controller as well as the analysis methods developed here are applicable to any robotic platform with a similar doubly-actuated spherical tail joint.

Disciplines

Electrical and Computer Engineering | Engineering | Systems Engineering

Frontal Plane Stabilization and Hopping with a 2DOF Tail

Garrett Wenger*

Avik De*

Daniel E. Koditschek*

Abstract—The Jerboa, a tailed bipedal robot with two hip-actuated, passive-compliant legs and a doubly actuated tail, has been shown both formally and empirically to exhibit a variety of stable hopping and running gaits in the sagittal plane. In this paper we take the first steps toward operating Jerboa as a fully spatial machine by addressing the predominant mode of destabilization away from the sagittal plane: body roll. We develop a provably stable controller for underactuated aerial stabilization of the coupled body roll and tail angles, that uses just the tail torques. We show that this controller is successful at reliably reorienting the Jerboa body in roughly 150 ms of freefall from a large set of initial conditions. This controller also enables (and appears intuitively to be crucial for) sustained empirically stable hopping in the frontal plane by virtue of its substantial robustness against destabilizing perturbations and calibration errors. The controller as well as the analysis methods developed here are applicable to any robotic platform with a similar doubly-actuated spherical tail joint.

I. INTRODUCTION

A large variety of animals possess and use inertial appendages to adjust their orientation. Fast reorientation is desired for reasons including agile maneuvers (rapid changes in heading) and protection from damage. For instance, bats use wings as inertial appendages, not just for aerodynamics [1], and monkeys with hands that are comparatively less adept at grasping use their tails inertially [2].

Reorientation is similarly important for robots to protect the hardware from damage. This has motivated a large recent literature in sagittal plane reorientation [3, 4]. In other areas of research, though the motivation is primarily facilitation of aggressive maneuvers [5, 6], similar ideas can be found underlying. In either case, “tails”—appendages with a small mass, but large inertia, frequently physically instantiated with a point mass at the tip of a long light link—can impart large reorientation effectiveness [3].

This work describes a reorientation controller implemented on the Penn Jerboa [7], a bipedal robot with a 2DOF actuated tail. The robot has 12 DOFs (6 body DOFs, 2 for the tail, and 2 per leg) and only 4 actuators (one on each hip and the remaining two driving the tail). As highlighted in [7], this unusual morphology supports a large number of steady [8] and transitional [9] locomotion tasks requiring both quasistatic and dynamic balance. In addition, the spherical tail joint allows the tail motors to exert a diversely oriented set of large moments and forces on the body, not in any way restricted to a preferred plane. We believe that this actuator will allow Jerboa to be a truly 3D

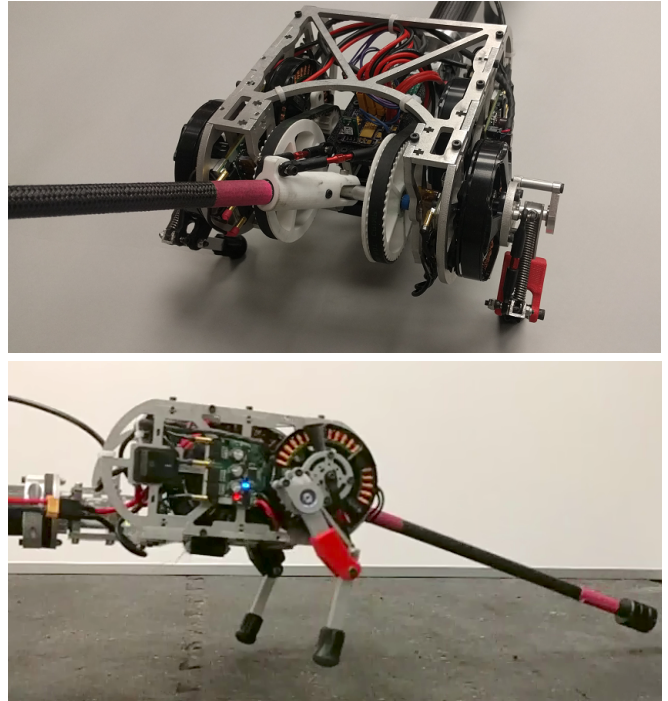


Fig. 1. In this paper, we develop a controller for the Penn Jerboa—a bipedal robot with a 2DOF tail [7]—to control its roll as well as tail configuration (3 DOFs) in flight using its two tail actuators. **Top:** A view of the Jerboa similar to the model in Fig. 2. **Bottom:** The experimental setup of the robot in aerial phase attached to a boom constraining pitch and yaw (but not roll). We empirically build on our roll controller to develop a stable tail-energized frontal plane hopping behavior (Section III).

machine, and in this paper we take the first steps out of the sagittal plane.

Sagittal reorientation capabilities have previously been demonstrated on this machine as a constituent behavior of planar hopping [8], however, as soon as the sagittally constraining boom is removed, even minor calibration errors and manufacturing differences in the leg springs, IMU, or hip motors can cause destabilizing rolling accelerations on the body (since it has very small rolling inertia). For some legged robots, small amounts of steady state roll have been shown to be beneficial [10]. However, based on experimental evidence, large roll instabilities are an impediment to 3D operation of the Jerboa and other robots [11] by reducing gait effectiveness or causing total failure. We seek to mitigate these instabilities by implementing a provably correct controller for this system and anticipate that the controller and analysis developed here will be useful for any robotic platform with a spherical 2DOF tail (e.g. [12, 13]). Previous work has shown that suitable controller constructions can

*Electrical and Systems Engineering, University of Pennsylvania, Philadelphia, PA, USA. {wenga, avik, kod}@seas.upenn.edu.

This work was supported in part by the ARL/GDRS RCTA project. Coop. Agreement #W911NF-10-2-0016 and in part by NSF grant #1028237.

compose actuated templates to control hopping [8]. Now, we aim to control body roll while simultaneously maintaining the mass center and sagittal plane stabilizing properties of these previously reported controllers.

In related spatial reorientation work [13], a 2DOF tail was effectively used to control body orientation in freefall. Contrasting with the present problem, in that work the final location of the tail was unimportant, and the controller could dissipate energy into the tail. For continuous hopping behavior built upon the previously developed controllers of [8], the Jerboa's tail must arrive at touchdown in a specified configuration. Consequently, this new work requires that we control additional DOFs with the same number of actuators when compared to [13].

The work in [14] aims to control the full configuration space of their robot, but stabilization of all the degrees of freedom is only possible after touchdown. In contrast, we wish to solve the underactuated stabilization problem in flight in order to facilitate tail-energized vertical hopping [8, Table II] upon touchdown.

In contrast to previous Jerboa work [8, 9, 15], roll is now the only body DOF considered in the configuration space, and the two tail motors appear as independently controlled torque sources (shown in Fig. 2 as connected to θ_y , θ_z). The overall contribution of this paper is a controller that provably stabilizes in flight the body roll and two tail DOFs of Jerboa using its two tail motors. We demonstrate this new controller both in simulation and empirically on the 3DOF boom-constrained Jerboa in freefall. Finally, we demonstrate empirically that this flight phase reorientation controller can be composed with the previously designed stance phase energy pumping controller to achieve stable frontal plane hopping with the Jerboa still affixed to the boom.

In Section II we outline the main theoretical contribution of this paper. In II-A, we employ a modeling approach similar to [4, 13] and identify a conserved quantity in the 3DOF flight dynamics (4), revealing kinematic equations of motion in the submanifold spanned by this constraint (6).

In II-B, we develop and prove stability for (Proposition 1) a novel (to the best of our knowledge) controller that stabilizes all of the DOFs in Fig 2 from a large basin of initial conditions. Note that this is possible in spite of the conservation law (4) because of the nature of the tail kinematics and their projection in the frontal plane.

In II-C we reconstitute this notional (velocity controlled) first order closed loop kinematic model as a target reference dynamics for the physical (torque-controlled) Jerboa frontal plane system. We again provide a proof that in spite of the underactuation, the two torque inputs can exponentially stabilize the velocity error in Proposition 2. We additionally propose a “natural” control variant (17) that is trivial to implement but has good performance in numerical (Fig. 3) and experimental (Fig. 6) trials.

Section III presents the experimental results, beginning with freefall trials of our novel controller of Section II in Figures 5–7. Next, we insert the reorientation control into the flight control strategy for frontal-plane hopping [8], and

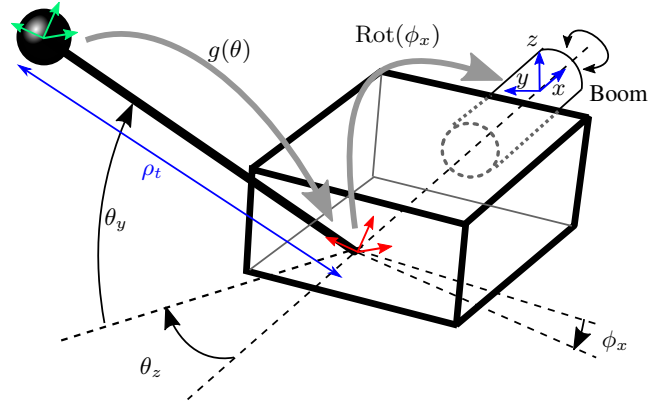


Fig. 2. Model for 3DOF reorientation of Jerboa in freefall (see Fig. 1 for the physical platform). Note that θ_y and θ_z are defined relative to the body orientation.

empirically show that it is crucial for sustained tail-energized hopping (Figures 8–10).

II. UNDERACTUATED ROLL AND TAIL STABILIZATION

A. Flight Kinematics

In the physical robot platform [7], the tail is a doubly actuated spherical joint whose kinematics can be parameterized by a “tail pitch” θ_y and “tail yaw” θ_z . Accordingly, the tail kinematics takes the form (see Fig. 2 for the location of the various configuration variables),

$$p_t := \rho_t \text{Rot}(\phi_x) g(\theta),$$

$$\text{where } g(\theta) = \text{Rot}(\theta_y) \text{Rot}(-\theta_z) \begin{bmatrix} -1 \\ 0 \\ 0 \end{bmatrix} = \begin{bmatrix} -c_y c_z \\ s_z \\ s_y c_z \end{bmatrix}, \quad (1)$$

where here (and throughout the paper), we use the shorthand c_y for $\cos \theta_y$, s_y for $\sin \theta_y$ etc.

The design of Jerboa deliberately places its CoM close to the hip (which is the origin of the tail joint (1)). Since the CoM behavior in freefall is trivial, we only pay particular attention to the orientation DOFs.

Additionally, for the physical demonstrations accompanying this research (Section III), the body yaw and pitch DOFs are locked, since we are first and foremost interested in roll stabilization. Thus, we consider the 3DOF system with the body roll and tail configuration, $q = (\phi_x, \theta_y, \theta_z)$. Additionally, for notational brevity, define $\theta = (\theta_y, \theta_z) \in S^1 \times S^1$. Please see Fig. 2.

With the system in freefall, there is no gravity in the frame that accelerates with the body's CoM, and the kinetic energy is

$$\kappa(q, \dot{q}) := \frac{1}{2} \left(i_b \dot{\phi}_x^2 + m_t \dot{p}_t^T \dot{p}_t \right) \quad (2)$$

where i_b is the body's moment of inertia about the x axis. Taking a derivative of (1) shows that $\dot{p}_t = \rho_t (\dot{\phi}_x J R g + R D g \dot{\theta})$, where $R := \text{Rot}(\phi_x)$, and J is the skew form of the ϕ_x -rotation, such that $\dot{R} R^T = \dot{\phi}_x J$. We can calculate

$$\kappa = \frac{i_t}{2} \left(\dot{\phi}_x^2 \left(\frac{i_b}{i_t} + g^T Q g \right) + 2 \dot{\phi}_x m^T \dot{\theta} + \dot{\theta}^T D g^T D g \dot{\theta} \right), \quad (3)$$

where $i_t = m_t \rho_t^2$, $m(\theta) := Dg^T Jg$, and $Q := R^T J^T J R = \text{diag}(0, 1, 1)$ is independent of ϕ_x . Thus, $\frac{\partial \kappa}{\partial \phi_x} = 0$, and since there is no external force directly on ϕ_x , by Noether's Theorem,

$$\alpha(q, \dot{q}) := \frac{\partial \kappa}{\partial \dot{\phi}_x} = (i_b + i_t g^T Q g) \dot{\phi}_x + i_t m(\theta)^T \dot{\theta}, \quad (4)$$

the ‘‘angular momentum,’’ is a conserved quantity.

B. Kinematic Reorientation

For this subsection, we proceed with the assumption that the tail velocities are a control input, i.e. we can set $\dot{\theta} = \omega$. This is useful

- a) in situations where the hardware is intrinsically designed for velocity control, or
- b) as the targetted (first order) reference dynamics [16] for a physical (second order) dynamical control system (which we describe in II-C).

If $\alpha(q, \dot{q}) = 0$ at $t = 0$ (zero initial angular momentum), then (4) can be rearranged to give the following kinematic equations of motion:

$$\dot{\phi}_x = -\frac{m^T}{i_b/i_t + g^T Q g} \omega \quad (5)$$

$$\dot{\theta} = \omega \quad (6)$$

Note that these equations are reminiscent of [4, (2)] and [13, (12)], which were derived under similar conditions by identifying the rate of change of angular momentum with 0. However, our conserved quantity (4) is different because of the distinct tail kinematics (Fig. 2) and their frontal plane projection. Define

$$w(\theta) := (-m_2(\theta), m_1(\theta)). \quad (7)$$

We choose the control input¹

$$\omega = m(\theta) k_1 \sin \phi_x + w(\theta) w(\theta)^T (-k_2 \theta) =: f(q). \quad (8)$$

Proposition 1. *Under the control (8), starting in the set $\theta \in \mathcal{G}$, a sufficiently small Euclidean ball around $\theta = 0$, the kinematic system (6) is asymptotically stable at $q = 0$.*

Proof. Define the potential

$$\varphi(q) := 1 - \cos \phi_x + \frac{1}{2} \theta^T \theta, \quad (9)$$

and note that under (8),

$$\begin{aligned} \dot{\varphi} &= \sin \phi_x \dot{\phi}_x + \theta^T \dot{\theta} \\ &= -\frac{k_1 m^T m \sin^2 \phi_x}{i_b/i_t + g^T Q g} - \theta^T (-m k_1 \sin \phi_x + k_2 w w^T \theta). \end{aligned}$$

Since $Q \succeq 0$, we have $g^T Q g \geq 0$, and so the first denominator is positive. Consequently, the first summand is nonpositive, and so

$$\begin{aligned} \dot{\varphi} &\leq -k_2 (\theta^T w)^2 + k_1 \sin \phi_x \theta^T m \\ &\leq -k_2 (\theta^T w)^2 + k_1 |\theta^T m| \end{aligned}$$

¹Note that if the initial angular momentum can be measured, it appears as an affine term in (5), and can be compensated for by modifying (8).

since $\sin \phi_x \leq 1$. In Appendix A we show that

$$\gamma(\theta) := \Gamma \cdot (\theta^T w)^2 - |\theta^T m| > 0 \quad (10)$$

in a sufficiently small Euclidean ball \mathcal{G} for $\Gamma \geq 1$ ². Setting $k_2 \geq \Gamma k_1$ ensures that $\dot{\varphi}|_{\mathcal{G}} < 0$. Moreover, note that we have in fact shown that $\frac{d}{dt}(\theta^T \theta) \leq 0$, and so the system remains in \mathcal{G} after starting in \mathcal{G} . \square

C. Velocity Target as Reference Dynamics

Now we can attempt to lift our target reference dynamics (8) to the dynamic tail-body system. From (3), we get the equations of motion

$$M \ddot{q} + C \dot{q} = \begin{bmatrix} 0 \\ \tau \end{bmatrix}, \quad (11)$$

where

$$M := \begin{bmatrix} i_b + i_t g(\theta)^T Q g(\theta) & i_t m(\theta)^T \\ i_t m(\theta) & i_t Dg(\theta)^T Dg(\theta) \end{bmatrix}. \quad (12)$$

In freefall, the conservation (4) still applies, and in particular its time derivative (6) can be rearranged to get the following constraint on velocities

$$\dot{q} = B(\theta) \dot{\theta}, \text{ where } B(\theta) := \begin{bmatrix} -\frac{m^T}{i_b/i_t + g^T Q g} \\ I_{2 \times 2} \end{bmatrix}. \quad (13)$$

Note that the equality above only holds when the initial angular momentum is zero. As we shall see in the proof of Proposition 2, this constraint makes the underactuated dynamic system (11) appear fully actuated when the task is tracking a reference velocity. Note that this is not as strong as stabilizing to a point (which is not possible with a smooth controller in an underactuated system [17]), we are simply stabilizing to a submanifold where the angular momentum is invariant.

With the desired reference velocity $f(q)$ from (8), define the velocity error

$$e := \dot{q} - Bf(q) = B(\dot{\theta} - f(q)) = B\bar{e} \quad (14)$$

where we additionally define $\bar{e} := \dot{\theta} - f(q)$ as the reduced θ -tracking error.

Proposition 2. *The controller*

$$\tau := -K\bar{e} + B^T \left(CBf + M \frac{d}{dt}(Bf) \right) \quad (15)$$

results in exponential convergence of $\dot{q} \rightarrow f(q)$ with rate controlled by K .

Proof. First, observe from (11) and (13) that $B^T \begin{bmatrix} 0 \\ \tau \end{bmatrix} \equiv \tau$, and so from (14), $e^T \begin{bmatrix} 0 \\ \tau \end{bmatrix} = \bar{e}^T \tau$. Define the energy function

$$\eta(q, \dot{q}) := \frac{1}{2} e^T M e, \quad (16)$$

²We show with numerical tools that even for $\Gamma = 1$, $\{\theta : \|\theta\| \leq 1\} \subset \mathcal{G}$.

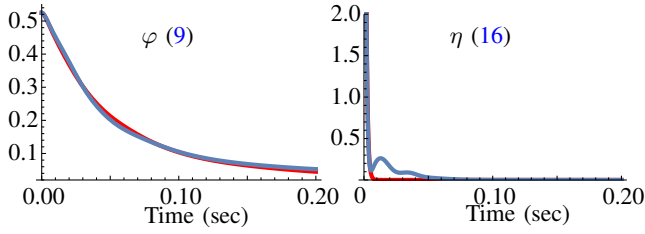


Fig. 3. Simulation results from identical initial conditions using the exact (15) (red) and natural (17) (blue) controllers. As expected from Proposition 2, η is monotonic in red, but we can see that the empirical performance of the natural control is sufficiently good, and in fact, almost indistinguishable in terms of the potential (9).

and note that

$$\begin{aligned}\dot{\eta} &= e^T \left(\frac{\dot{M}}{2} e + M \dot{e} \right) \\ &= e^T \left(\frac{\dot{M}}{2} e + M \ddot{q} - M \frac{d}{dt}(Bf) \right) \\ &= e^T \left(\frac{\dot{M}}{2} e + \begin{bmatrix} 0 \\ \tau \end{bmatrix} - C(e + Bf) - M \frac{d}{dt}(Bf) \right) \\ &= e^T \left(\left(\frac{\dot{M}}{2} - C \right) e + e^T \left(\begin{bmatrix} 0 \\ \tau \end{bmatrix} - CBf - M \frac{d}{dt}(Bf) \right) \right),\end{aligned}$$

where the first summand will disappear since $\dot{M} - 2C$ is skew symmetric [16]. Additionally, we can use (14) to see that

$$\dot{\eta} = \bar{e}^T \left(\tau - B^T C B f - B^T M \frac{d}{dt}(Bf) \right) = -\bar{e}^T K \bar{e}$$

using (15). Thus $\eta \rightarrow 0$ exponentially fast, and so does e using (16). \square

Remark 1 (Natural control). The controller (15) cancels some velocity dependent terms (the $B^T(\dots)$ terms), but in simulation and experiments we have found that the more “natural” [16] control

$$\tilde{\tau} := -K \bar{e} \quad (17)$$

results in empirically good performance, and it is used in all of Section III. In Fig. 3 we have included simulation traces from identical initial conditions using both forms of the controller.

D. Application to Hopping

We provided empirical evidence in [8] that a parallel composition of a tail-energized vertical hopping with controllers to coordinate sagittal body and tail angles can produce a planar hopping behavior. We are now interested to see if a similar idea can produce frontal plane hopping (leading up to—after appropriate composition with the sagittal plane controllers—3D hopping).

For tail-energized vertical hopping, it is crucial for the tail position to be controlled in flight, so as to allow for a desired stance initial condition [15]. Together with the angular momentum constraint (4), this leaves us with an underactuated stabilization problem in flight, which motivated the development of our novel controller (15). When

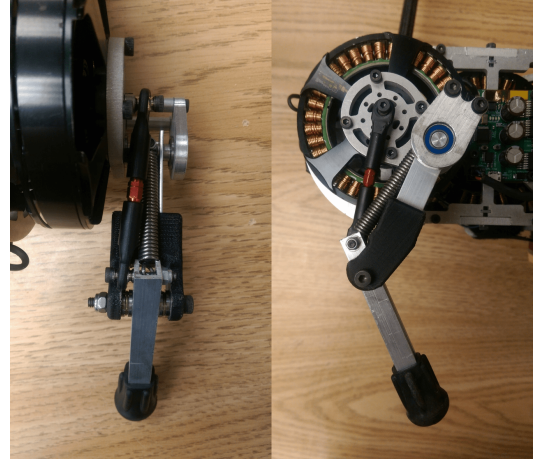


Fig. 4. The redesigned Jerboa legs (compared to [7]) with large improvements in frontal plane stiffness, but not much added rotational inertia about the hip, through use of added bearings and joint supports and more robust material composition overall.

TABLE I
PENN JERBOA [7] PARAMETERS

Mass (with battery)	2.419 Kg
Dimensions (without tail)	0.21 m (L) \times 0.23 m (W) \times 0.1 m (H)
Tail length	0.4 m
Tail mass	150 g

employed during hopping, an added consideration is the amount of time required to stabilize. Proposition 1 is only an asymptotic result and does not provide bounds on completion time. However, through the empirical testing in III, we have determined that the controller stabilizes the body roll fast enough to be used in tandem with tail-energized vertical hopping [8, Table II].

Additionally, the frontal plane hopping behavior involves both legs, unlike the sagittal projection [8, 15]. We suspect that near-simultaneous touchdowns benefit from a hybrid stabilization effect [18]. However, without appropriate roll control (akin to touchdown synchronization between the two legs), the unmodeled single-stance dynamics can play a large role (see, for example, Fig. 10).

III. EXPERIMENTAL RESULTS

For the experimental setup, the constraining boom is mounted below the robot’s center of mass, which has no effect during freefall but is slightly destabilizing during hopping. Thus, the results presented in Section III-B are representative of a ‘worst case’ scenario where the body roll is being perturbed in a way that does not occur if the robot is unconstrained. Roll data comes from a Kalman filtered IMU, tail angles are calculated according to the tail linkage using magnetic encoder position data, and body height is measured using an IR distance sensor mounted underneath the robot.

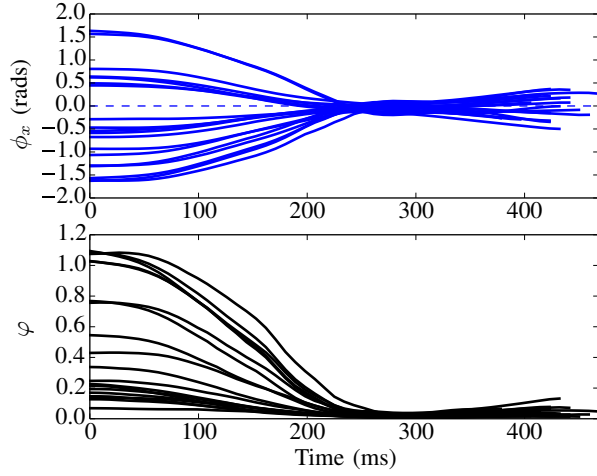


Fig. 5. Body roll and potential ϕ from 20 freefall reorientation trials. The stabilization time is roughly consistent across a wide range of initial roll angles.

A. Reorientation in Flight

For each freefall trial, the robot drops from a height of roughly 1.5 m with a varied roll angle and no initial angular velocity. When the robot detects that it is in freefall based on IMU readings, it uses the simple velocity controller in (17) and the input from (8) to reorient and stabilize the body pitch and tail angles. Both legs were removed during these experiments for convenience, but since they have no function during flight and make up only a small percentage of the total mass (under 10%), this should not impact reorientation performance significantly.

Fig. 5 shows roll data from a collection of 20 trials. The system stops recording data when it measures an acceleration spike (indicating ground contact), which, coupled with the approximated drop height, explains the slight variation in trial length. There is some noticeable overshoot and oscillation that is likely caused by delay from the roll Kalman filter and overall accuracy of the motor velocity controller. However, because the Jerboa has such a short aerial phase while hopping, the speed at which large changes can be corrected is more important than long term stability.

The plots in the right column of Fig. 6 display additional data from one of the trials in Fig. 5. We observe that the empirical behavior bears marked resemblance to simulation results from the same initial conditions (left column of Fig. 6). In either case, all three of the system's DOFs are driven to their desired values well within the drop time. The tail angles follow roughly sinusoidal trajectories with decaying amplitude that are out of phase by about 90 degrees. This equates to the tail spiraling inwards to the center of a cone—though the controller (Section II) is purely feedback driven with no trajectory planning involved.

B. Tail-energized Frontal-plane Hopping

1) *Hardware modifications:* During hopping, the Jerboa legs are subject to significant out-of-plane bending moments if the robot lands with nonzero roll angle. The original

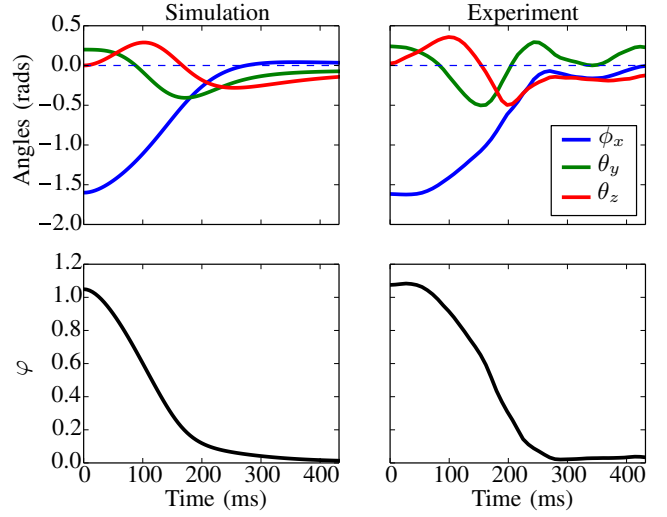


Fig. 6. A detailed view of the controlled configuration angles (top) and potential function ϕ (bottom) defined in (9) in simulation (left) and during a reorientation trial (right) with the same initial conditions. The majority of the stabilization occurs in 150 ms.

legs used for sagittally constrained hopping [7, 15] were not designed for this purpose and either deformed or broke under these loads. This (a) provides additional motivation for this research project, since roll reorientation can avoid this hardware failure mode, and (b) led us to design new legs with significantly more stiffness in the frontal plane. Fig. 4 shows the mechanical design of the new legs. This new design separates the toes slightly more than before, increasing the moment due to gravity in single support. Further, the added rigidity of the legs dissipates more kinetic energy when touchdown occurs with non-zero roll. These two factors are beneficial for hopping as they give the system some amount of passive stability.

2) *Empirical results:* To test continuous hopping, the Jerboa drops from roughly 2 leg lengths with minimal initial roll angle. Data collection starts once the transients from the initial drop diminish. These trials were conducted with the roll controller both enabled and disabled. In all cases, the trials ended before failure as a precaution against motors overheating.

The lower plot in Fig. 8 shows baseline performance of the hopping controller from [15]. While this controller was not designed to work when the robot is free to roll, it does still enable prolonged, steady state hopping. There are many sources of error that can destabilize the body roll during hopping, including unmatched leg springs, slight differences in leg touchdown time, noise in the motor control loop, and external disturbances. With the roll controller disabled, only the passive stability that comes from the legs acts against these destabilizing factors. Indeed, the robot does hop stably for some time, which can be seen for the first 7.5s of the referenced figure. However, once it becomes significantly unstable, it does not recover fully.

In the upper plot, where the roll controller is enabled, the jump height and roll are much more consistent. Apex



Fig. 7. Frames from a single reorientation trial showing that the tail can correct a large initial roll angle. In the projection onto the coronal plane, the tail spirals inwards in the clockwise direction. Between frames 4 and 5, the tail moves back to the reset position at $(\theta_y, \theta_z) = (0, 0)$ once roll has been brought to near 0.

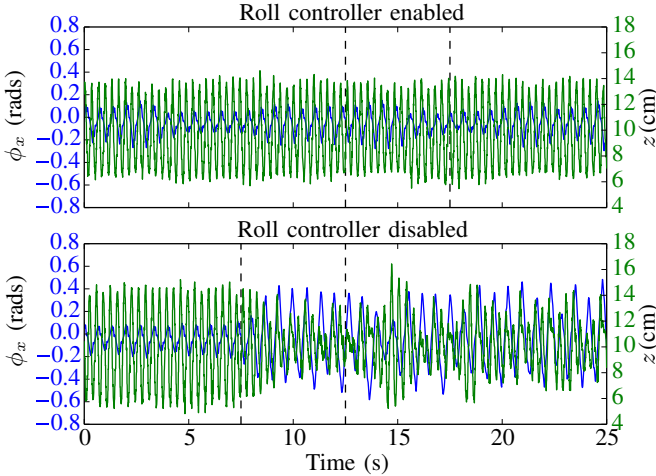


Fig. 8. Steady state hopping with the proposed roll controller enabled (top) and disabled (bottom). While both figures show periods of stability, once hopping without roll control enabled becomes unstable, it does not recover. The robot was not externally disturbed at any time during these trials. The sections between the vertical dashed lines are shown in detail in Fig. 9.

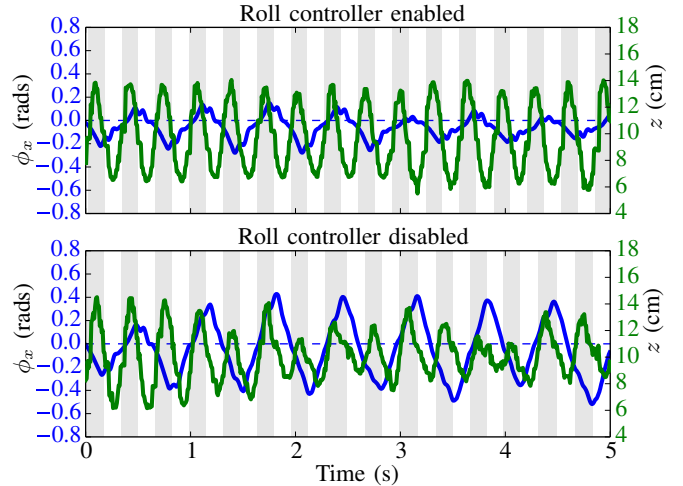


Fig. 9. An enlarged view of roll angle (blue) and height (green) during steady state hopping with the roll controller enabled (top) and disabled (bottom). The white and grey background represent periods when the robot was in stance and flight, respectively. At 2.2s, the long flight phase is a result of the robot being supported by the constraining boom while nearly flipping, which can be considered a failure even though hopping does resume.

hopping height shows some minor amplitude fluctuation and the roll exhibits oscillations on the order of ± 0.2 radians around 0 (since the controller is only asymptotically stable, small roll errors are not corrected in a very short amount of time), but the controller manages to prevent any larger roll excursions.

Finally, note that Fig. 8 shows the oscillating height of the robot's COM over a 25 second period, which would be more than enough time for these hopping oscillations to die out if nothing was energizing the system. For frontal plane hopping, only the tail motors are performing any active control. While the legs are enabled, those motors are merely holding position, and so they do not contribute to the energization of the leg springs. Thus, it is clear that the tail is successfully serving as both an energy pump [15] and inertial appendage.

IV. CONCLUSIONS AND FURTHER WORK

In this paper, we introduce a provably stable kinematic controller for underactuated frontal plane reorientation, and implement it on a dynamic robot platform using a provably stable target dynamics tracking controller. A “natural control” variant of this controller is demonstrated to be

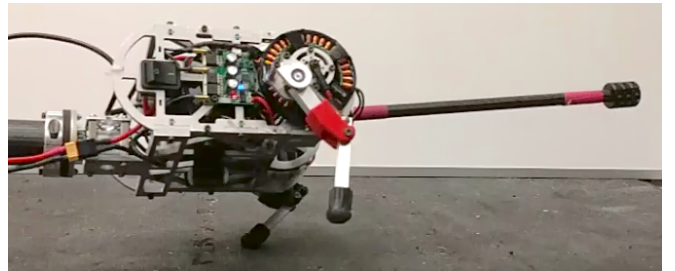


Fig. 10. A snapshot from the long ‘flight’ phase described in Fig. 9. Flight is estimated based on readings from a downwards facing IR sensor. In this case, the robot rolled enough while beginning to hop that this single contact stance initiates the flight controller.

successful both in simulation and experiments even though it does not cancel the system's natural dynamics. Further, this controller is combined with a previously documented hopping controller [8], and we show experimentally that the hopping behavior is improved by the in-flight roll stabilization provided by the kinematic controller.

Future work will initially focus on analyzing the composition of these controllers using methods similar to [15].

Beyond this, we aim to combine the shape and stepping controllers from [8] with the work in this paper to enable untethered spatial hopping with the Jerboa.

REFERENCES

- [1] A. Bergou, S. Swartz, H. Vejdani, D. Riskin, L. Reimnitz, G. Taubin, and K. Breuer, “Falling with style: Bats perform complex aerial rotations by adjusting wing inertia,” *PLoS Biology*, vol. 13, no. 11, 2015. 1
- [2] J. Young, G. Russo, C. Fellmann, M. Thatikunta, and B. Chadwell, “Tail function during arboreal quadrupedalism in squirrel monkeys (*saimiri boliviensis*) and tamarins (*saguinus oedipus*),” *Journal of Experimental Zoology Part A: Ecological Genetics and Physiology*, vol. 323, no. 8, pp. 556–566, 2015. 1
- [3] T. Libby, T. Y. Moore, E. Chang-Siu, D. Li, D. J. Cohen, A. Jusufi, and R. J. Full, “Tail-assisted pitch control in lizards, robots and dinosaurs,” *Nature*, vol. 481, no. 7380, pp. 181–184, Jan. 2012. 1
- [4] A. M. Johnson, E. Chang-Siu, T. Libby, M. Tomizuka, R. J. Full, and D. E. Koditschek, “Tail assisted dynamic self righting,” in *Proceedings of the International Conference on Climbing and Walking Robots*, 2012. 1, 2, 3
- [5] A. O. Pullin, N. J. Kohut, D. Zarrouk, and R. S. Fearing, “Dynamic turning of 13 cm robot comparing tail and differential drive,” in *2012 IEEE International Conference on Robotics and Automation (ICRA)*. IEEE, 2012, pp. 5086–5093. 1
- [6] A. Patel and M. Braae, “Rapid acceleration and braking: Inspirations from the cheetah’s tail,” in *2014 IEEE International Conference on Robotics and Automation (ICRA)*, May 2014, pp. 793–799. 1
- [7] A. De and D. E. Koditschek, “The Penn Jerboa: A Platform for Exploring Parallel Composition of Templates,” *Technical report. arXiv preprint arXiv:1502.05347*, 2015. 1, 2, 4, 5
- [8] —, “Parallel composition of templates for tail-energized planar hopping,” in *2015 IEEE International Conference on Robotics and Automation (ICRA)*, May 2015, pp. 4562–4569. 1, 2, 4, 6, 7
- [9] A. L. Brill, A. De, A. M. Johnson, and D. E. Koditschek, “Tail-assisted rigid and compliant legged leaping,” in *Intelligent Robots and Systems (IROS), 2015 IEEE/RSJ International Conference on*. IEEE, 2015, pp. 6304–6311. 1, 2
- [10] S. Burden, J. Clark, J. Weingarten, H. Komsuoglu, and D. E. Koditschek, “Heterogeneous leg stiffness and roll in dynamic running,” in *Proceedings of IEEE Conference of Robotics and Automation*, 2007. 1
- [11] H. G. Kim, D. G. Lee, and T. W. Seo, “Rolling Stability Enhancement via Balancing Tail for a Water-running Robot,” *Journal of Bionic Engineering*, vol. 12, no. 3, pp. 395–405, 2015. 1
- [12] A. Patel and E. Boje, “On the conical motion of a two-degree-of-freedom tail inspired by the cheetah,” *IEEE Transactions on Robotics*, vol. 31, no. 6, pp. 1555–1560, Dec 2015. 1
- [13] E. Chang-Siu, T. Libby, M. Brown, R. J. Full, and M. Tomizuka, “A nonlinear feedback controller for aerial self-righting by a tailed robot,” in *Robotics and Automation (ICRA), 2013 IEEE International Conference on*. IEEE, 2013, pp. 32–39. 1, 2, 3
- [14] J. T. Bingham, J. Lee, R. N. Haksar, J. Ueda, and C. K. Liu, “Orienting in mid-air through configuration changes to achieve a rolling landing for reducing impact after a fall,” in *2014 IEEE/RSJ International Conference on Intelligent Robots and Systems (IROS)*, Sept 2014, pp. 3610–3617. 2
- [15] A. De and D. E. Koditschek, “Averaged Anchoring of Decoupled Templates in a Tail-Energized Monoped,” in *2015 International Symposium on Robotics Research*, Sept. 2015. 2, 4, 5, 6
- [16] D. E. Koditschek, “Adaptive techniques for mechanical systems,” in *Proc. 5th. Yale Workshop on Adaptive Systems*, May 1987, pp. 259–265. 3, 4
- [17] M. W. Spong, “Underactuated mechanical systems,” in *Control Problems in Robotics and Automation*. Springer-Verlag, 1998. 3
- [18] S. A. Burden, S. Revzen, S. S. Sastry, and D. E. Koditschek, “Event-selected vector field discontinuities yield piecewise-differentiable flows,” *SIAM Journal on Applied Dynamical Systems*, vol. 15, no. 2, pp. 1227–1267, 2016. 4

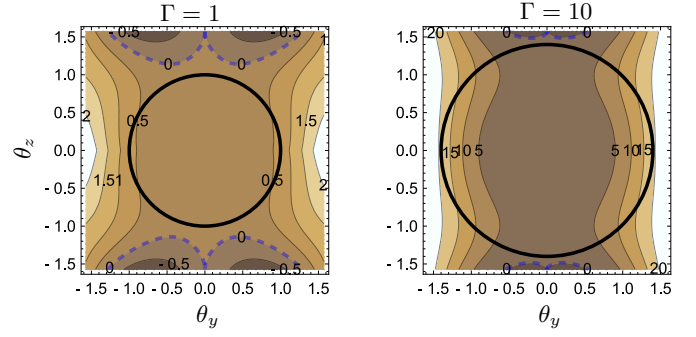


Fig. 11. In these contour plots of the scalar valued function (10), the 0 level is highlighted with the dashed blue curve. As Γ is changed from 1 to 10, \mathcal{G} can be increased in size from $\|\theta\| \leq 1$ (left) to $\|\theta\| \leq 1.4$.

APPENDIX

A. Proof of (10)

First, we note that $\gamma : S^1 \times S^1 \rightarrow \mathbb{R}$ has a single parameter, Γ . In Fig. 11 we show numerically that (a) (10) has the sign property we want, and (b) the size of \mathcal{G} can be tuned by the parameter Γ . Fig. 11 shows that for $\Gamma = 1$, \mathcal{G} at least includes the ball $\|\theta\| \leq 1$, and that increasing Γ increases the potential size of \mathcal{G} further.

In addition, we can also see using a second-order Taylor approximation that close to the origin $\theta = 0$, the sign property still holds (though to estimate the size of \mathcal{G} , we still have to use Fig. 11). From (1), we can calculate

$$m(\theta) = \begin{bmatrix} c_y c_z s_z \\ -s_y \end{bmatrix}, \quad (18)$$

and consequently

$$w^T \theta = s_y \theta_y + c_y c_z s_z \theta_z, \quad m^T \theta = c_y c_z s_z \theta_y - s_y \theta_z.$$

Using the second-order Taylor expansions for sin and cos, $\gamma(\theta)$ can be approximated as

$$\begin{aligned} \tilde{\gamma}(\theta) = & \left(\frac{1}{4} (2 - \theta_y^2) (2 - \theta_z^2) \theta_z^2 + \theta_y^2 \right)^2 \\ & - \left| \frac{1}{4} \theta_y \theta_z (4 - (2 - \theta_y^2) (2 - \theta_z^2)) \right|. \end{aligned}$$

This approximated form is symmetric ($\tilde{\gamma}(\theta_y, \theta_z) = \tilde{\gamma}(-\theta_y, \theta_z) = \tilde{\gamma}(\theta_y, -\theta_z) = \tilde{\gamma}(-\theta_y, -\theta_z)$) across all quadrants, and so only its behavior in the first quadrant needs to be considered. With this restriction (and close to the origin, where this approximation is relevant), the term inside the $|\cdot|$ is non-negative, allowing the absolute value to be dropped. Now it is possible to rearrange terms such that

$$\begin{aligned} \tilde{\gamma}(\theta) = & \left(\frac{1}{4} (2 - \theta_y^2) (2 - \theta_z^2) \theta_z^2 + \theta_y^2 \right)^2 \\ & - \frac{1}{4} \theta_y \theta_z (4 - (2 - \theta_y^2) (2 - \theta_z^2)) \\ = & 2\theta_y^2 \theta_z^2 + \mathcal{O}(\theta_y^3) + \mathcal{O}(\theta_z^3) \end{aligned}$$

and so positivity of (10) near the origin is verified, as desired.